Electronic Supplementary Material (ESI) for Nanoscale.

Supplementary Information for Mechanical Conductance Tunability of a Porphyrin-Cyclophane Single-Molecule Junction

Werner M. Schosser,[†,#] Chunwei Hsu,[‡,#] Patrick Zwick,[¶,#] Katawoura Beltako,[†] Diana Dulić,[§] Marcel Mayor,[*,¶,‖,⊥,@] Herre S. J. van der Zant,[*,‡,@] and Fabian Pauly[*,†,@]

†*Institute of Physics, University of Augsburg, 86135 Augsburg, Germany*

‡*Kavli Institute of Nanoscience, Delft University of Technology, Lorentzweg 1, Delft 2628 CJ, The Netherlands*

¶*Department of Chemistry, University of Basel, St. Johanns-Ring 19, 4056 Basel, Switzerland*

§*Department of Physics, Department of Electrical Engineering, Faculty of Physical and Mathematical Sciences, University of Chile, Avenida Blanco Encalada 2008, Santiago 8330015, Chile*

‖*Institute for Nanotechnology (INT), Karlsruhe Institute of Technology (KIT), P. O. Box 3640, 76021 Karlsruhe, Germany*

⊥*Lehn Institute of Functional Materials (LIFM), School of Chemistry, Sun Yat-Sen University (SYSU), 510275 Guangzhou, China*

#*These authors contributed equally.*

@*Corresponding authors.*

E-mail: marcel.mayor@unibas.ch; h.s.j.vanderzant@tudelft.nl; fabian.pauly@uni-a.de

Contents

In the main text, we present the conduction properties of PC1 molecular junctions. This part focuses mostly on the behavior of the ZnPC1 derivative, see Fig. 2.

ESI.1 Theoretical

ESI.1.1 DFT and electronic transport simulations for ZnPC1

The DFT and electronic transport simulations to determine the properties of ZnPC1 molecular junctions are performed in exactly the same way, as described in the Methods section of the main text. This includes the use of the same computational parameters.

ESI.1.2 Junction evolution and electronic transport for ZnPC1

Let us discuss the geometrical evolution of the ZnPC1-based single-molecule junction during the stretching process, presented in Fig. S1, which proceeds similarly to the PC1 junction described in the main text. The junction evolution is reflected in the behavior of the total energy and the conductance, shown in Fig. S2, which we will discuss at the same time.

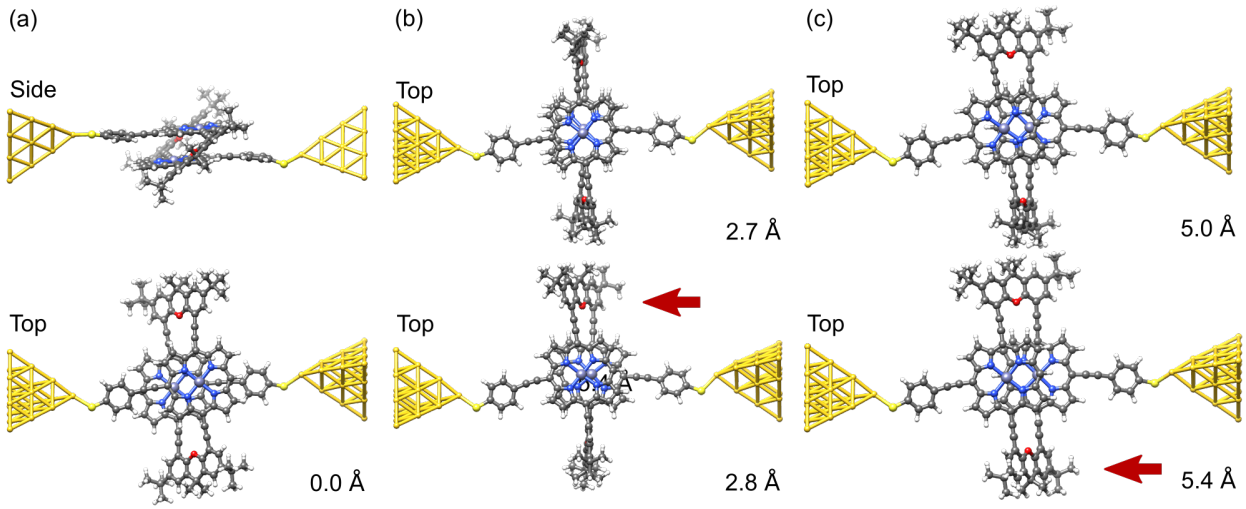

Figure S1 (a) Side and top views of the ZnPC1 molecule between two gold electrodes at an electrode displacement of $d = 0$ Å. Snapshots illustrating (b) the first bridge flip at around 2.7 Å and (c) the second bridge flip. The second bridge flip occurs rather continuously over an electrode displacement interval ranging from around 5.2 Å to 5.6 Å. Red arrows indicate the bridge that flips.

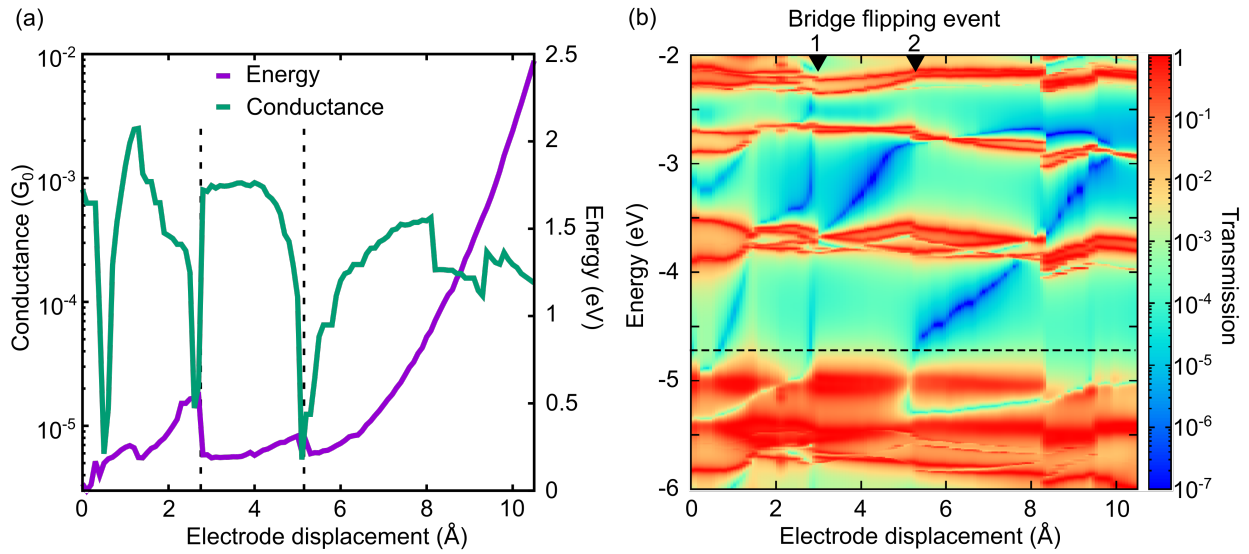

Figure S2 (a) Energy and low-temperature conductance $G_0\tau(E_\mathrm{F})$ as a function of electrode displacement for the simulated ZnPC1 molecular junction. (b) Transmission as a function of electrode displacement and energy. Horizontal red resonances arise from molecular frontier orbitals. Tunable DQI effects, observed inside the HOMO-LUMO gap, shift in energy as the displacement is varied. Black triangles mark the first and second bridge flipping events. The position of the Fermi energy $E_\mathrm{F} = -4.69$ eV is indicated as a horizontal dashed line in the plot. The conductance curve of panel (a) is obtained by tracing the transmission map along E_F.

Starting at zero electrode displacement in the compressed molecular state, the two porphyrin planes slide over each other in parallel. After a slight geometrical reconfiguration at 1.5 Å, visible as small decrease in total energy in Fig. S2a, the first xanthene bridge is flipped at 2.7 Å. This point coincides with a sharp decrease in the DFT total energy. The flip of the bridge causes porphyrin planes to twist, when we look at ZnPC1 from the top, see Fig. S1b. The twisted porphyrin plane configuration is energetically favored from this point onward until the second bridge flips at around 5.2 Å, see Fig. S1c. Note, however, that the second bridge flip does not happen as instantaneously as the first, but rather gradually in a transition region from around 5.2 Å to 5.6 Å. From this point onwards the twist of the porphyrin planes is basically removed, and they are again well aligned, when seen from the top, see Fig. S1c. Between 5.6 Å and 10.5 Å, the porphyrin planes slide over each other, building up more and more tension in the molecule as the energy rises, see Fig. S2a. Finally, the junction breaks at 10.5 Å, when the molecule loses contact to one of the electrodes as the

mechanical tension becomes too high. As a results, the conductance drops to zero sharply.

During the stretching process, the conductance of the ZnPC1 junction shows sharp dips at 0.5 Å, and in the vicinity of the first and second bridge flipping events at 2.7 Å and 5.2 Å, see Fig. S2a. Conductance changes around 8.2 Å and 9.3 Å can be related to a pronounced intramolecular sliding motion of the porphyrin planes.

In the contour map of transmission as a function of electrode displacement and energy, see Fig. S2b, sudden geometric rearrangements lead to a discontinuous distance dependence. Such discontinuities are visible at 1.5 Å, 2.8 Å, 5.2 Å, 8.2 Å and faintly at 9.3 Å. Inside the electronic gap between the HOMO and the LUMO, the ZnPC1 junction shows transmission valleys (blue diagonal traces) with transmission values ranging down to 10^{-7}, causing DQI conductance dips. The dips in the conductance-distance trace of Fig. S2a at 0.5 Å, 2.7 Å and 5.2 Å are all caused by crossings of the Fermi energy with such DQI features in Fig. S2b.

A comparison of Fig. S2 for ZnPC1 with Fig. 4 for PC1 reveals a similar transport behavior of both molecular junctions. As a main difference, the dip at the first bridge flipping event at 2.7 Å is more pronounced for ZnPC1 than for PC1. Otherwise, the contour plots of the transmission show very similar valleys and resonance features, as expected from the comparable molecular structure. In summary, this further solidifies the hypothesis of the central porphyrin subunit as the origin of the DQI phenomenona.

ESI.1.3 Quantum interference effects and orbital symmetry rules for ZnPC1

The blue valleys of suppressed transmission inside the HOMO-LUMO gap for PC1 molecular junctions in Fig. 4b arise from DQI effects. As discussed in the main text, they can be related to the contributions of gas phase frontier molecular orbitals, see Fig. 5.[1]

Let us now understand in a similar way the DQI features for the ZnPC1 molecular junction, which are visible in Fig. S2. Figure S3 shows the relevant frontier molecular orbital wavefunctions at different electrode displacements. The displacements are chosen such that

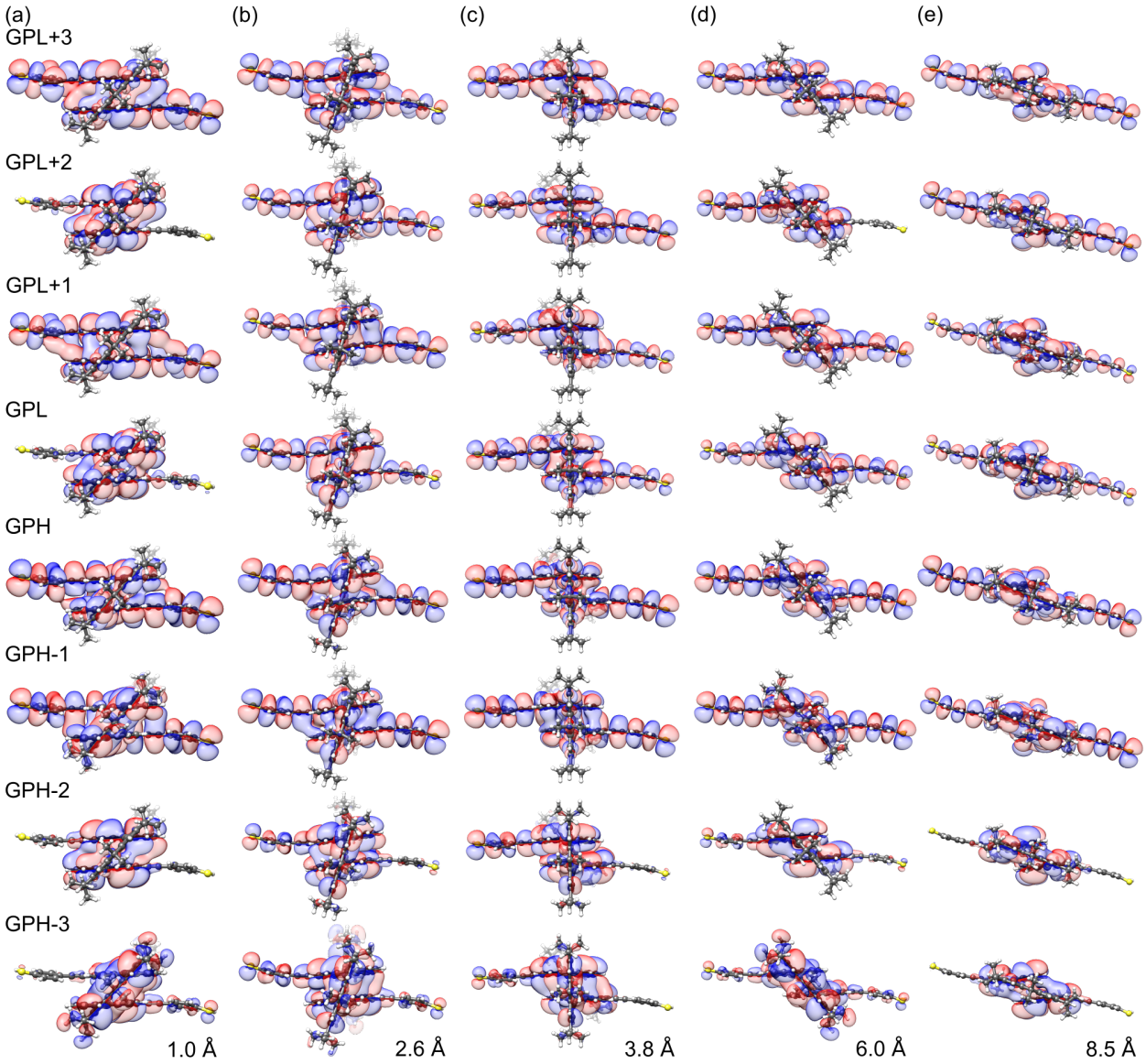

Figure S3 Frontier molecular orbitals of the ZnPC1 molecule in the gas phase for different electrode displacements d. Shown are the gas phase HOMO (GPH) and gas phase LUMO (GPL) together with the energetically nearest orbitals GPH$-n$ and GPL$+n$ with $n = 1, 2, 3$.

the regions from around 0 Å to 1.5Å, 1.6 Å to 2.0Å, 2.0 Å to 2.7 Å, 2.8 Å to 5.2 Å, 5.3 Å to 8.2 Å and 8.3 Å to 10.5 Å, which show similar DQI effects in the transmission map of Fig. S2b, are well characterized. From Fig. S3 the weights on terminal sulfurs as well as the parity of the orbitals can be read off, which are needed to rationalize the transport behavior in terms of orbital symmetry rules.[1] Orbital wavefunctions all show a p-like character with a comparable orientation on the terminal sulfur atoms or a vanishing weight, as required. As in the main

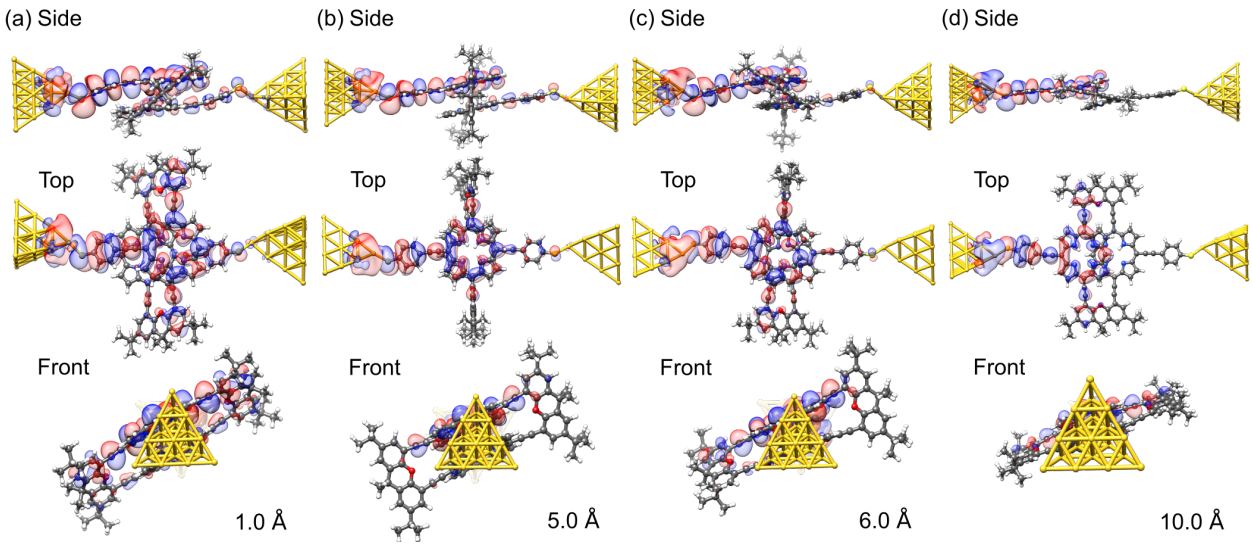

Figure S4 Side, top and front views of the wave functions of left-incoming transmission eigenchannels for electron transport through the PC1 molecule connected to gold electrodes. The most transmissive eigenchannel is shown at the Fermi energy for different electrode displacements of (a) $d = 1.0$ Å, (b) 5.0 Å, (c) 6.0 Å, and (d) 10.0 Å.

text, we find it sufficient to argue only with a single occupied and unoccupied orbital pair to explain the presence or absence of DQI inside the HOMO-LUMO gap. At an electrode displacement of 1.0 Å, the GPL shows vanishing weight on the terminal sulfur atoms, so that we concentrate on the GPH and GPL+1. They show the same parity, leading to the presence of DQI in the corresponding region from 0 Å to 1.5 Å. Similarly, GPH and GPL at 2.6 and 6.0 exhibit the same parities, leading to DQI in the regions 2.0 Å to 2.7 Å, and 5.3 Å to 8.2 Å. On the other hand, the orbitals GPH and GPL at 1.8 Å (not shown), 3.8 Å, and 8.5 Å, respectively, have different parity, causing DQI to be absent in the corresponding displacement regions. We have thus related the DQI effects to energetic rearrangements of HOMO and LUMO orbitals, which are controlled by the mechanical manipulation of the ZnPC1 molecule during the stretching process.

ESI.1.4 Transmission eigenchannels

Figures S4 and S5 visualize left-incoming transmission eigenchannels at the Fermi energy for PC1 and ZnPC1, respectively. As can be seen, the amplitude of the eigenchannels decays

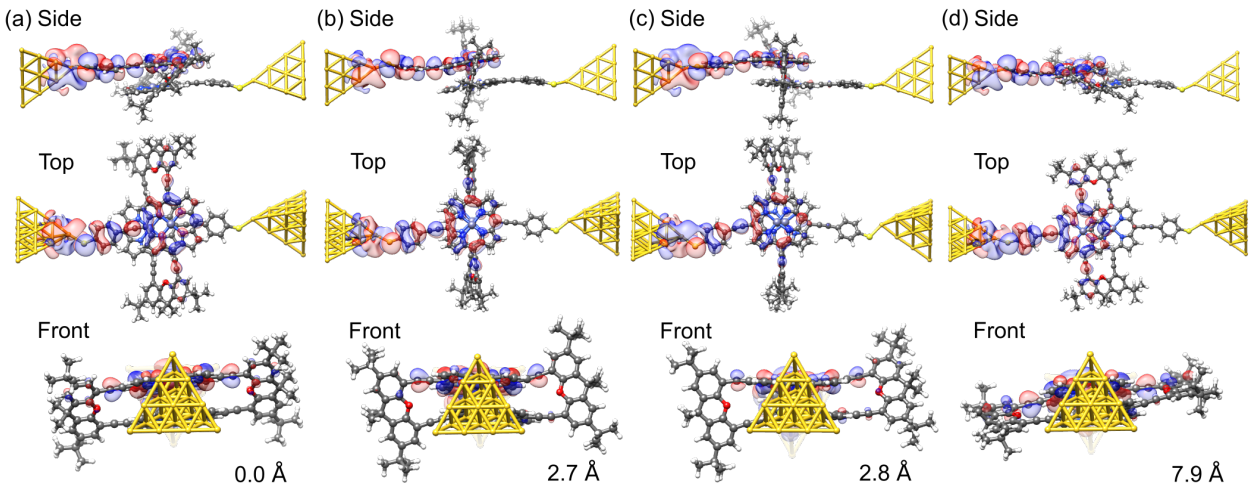

Figure S5 Same as Fig. S4 but for ZnPC1. The most transmissive eigenchannel is shown at the Fermi energy for different electrode displacements of (a) $d = 0$ Å, (b) 2.7 Å, (c) 2.8 Å, and (d) 7.9 Å.

along the propagation direction within the molecules, as it is typical for an off-resonant transport situation. Overall, the spatial distribution of the wavefunctions shows a high weight on the molecular deck directly connected via a sulfur anchor to the left electrode and a low weight on the molecular deck directly connected to the right electrode, as expected. The transmission eigenchannels reveal that the planar bridging xanthene units and revolving acetylene joints are involved in transport as well. This means that the electron transport through the molecule proceeds both through space, directly from one porphyrin ring to the other, but also through bond, i.e. through the bridges. Interestingly, the electric transport through bond depends on the stretching state of the molecule. The overlap of electronic π-systems is large, when bridges align well with the porphyrin decks. This is the case in compressed or stretched molecular states. In contrast, in the intermediate region close to bridge flipping events, when bridges are nearly perpendicular to the porphyrin decks, π-orbitals of decks and bridges are perpendicular, the electronic overlap is small or vanishes, and transport through bond is largely suppressed, see for instance the situation at $d = 5.0$ Å in Fig. S4 or at $d = 2.7$ Å in Fig. S5. From the plots, it is obvious that both PC1 and ZnPC1 show an analogous behavior.

ESI.1.5 Quantification of through-space and through-bond transport contributions

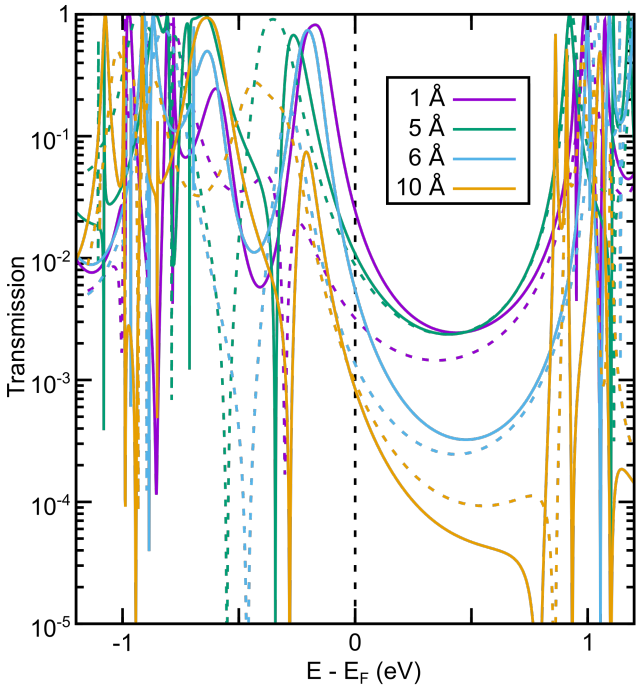

Figure S6 Transmission as a function of energy for electrode displacements, corresponding to those shown in Fig. S4. The solid curves are obtained as vertical cuts in the transmission map of Fig. 4b for the simulated Au-PC1-Au junction. The dashed curves are for molecular contacts, where the two xanthene bridges and four acetylene joints are replaced by four hydrogen atoms, each positioned at one of the acetylene attachment points.

The transmission eigenchannels in Figs. S4 and S5 show that the xanthene bridges yield a finite through-bond contribution to transport in addition to the through-space part from the direct tunneling between the porphyrins. In order to quantify how these transport contributions depend on the stretching state, we compare in Fig. S6 the transmission curves for the full Au-PC1-Au junctions, discussed in Figs. 3 and 4 of the main text, with the same geometries but removed xanthene bridges and acetylene joints. In the latter case single hydrogen atoms are saturating those carbons, where acetylene joints are connected in the PC1 molecule. The modified molecular junction geometries without joints and bridges are not optimized, in order to ensure an optimal comparability to the original PC1 contacts.

The transmission curves as a function of energy at different electrode displacements d are shown in Fig. S6. Solid lines correspond to vertical cuts in Fig. 4b of the main text, whereas the dashed transmission curves are for those, where bridges and joints are removed. Since solid curves are generally higher than dashed ones within the HOMO-LUMO gap, except for the very extended junction state of $d = 10$ Å, exhibiting a rather low transmission, the bridges tend to increase the transmission. When the overlap of electronic π-systems is large at $d = 1$ Å, i.e. when bridges align well with the porphyrin decks, the transmission enhancement is largest and amounts to nearly an order of magnitude at the Fermi energy. In contrast, when π-orbitals of porphyrin decks and bridges are nearly perpendicular at $d = 5$ Å, the through-bond contribution of the bridges vanishes, and dashed and solid lines almost coincide.

Overall, our analysis shows that the changes in the transmission at the Fermi energy $\tau(E_{\mathrm{F}})$, resulting from a removal of through-space bridge contributions, are smaller than the four orders of magnitude modulation observed during junction stretching in Fig. 4 of the main text. The mechanosensitivity of the PC1 molecule is based on DQI effects, and our argumentation with the gas phase molecular orbitals in Fig. 5 of the manuscript takes into account both through-space and through-bond parts.

ESI.1.6 Robustness of the energetic ordering of frontier molecular orbitals

In order to inspect the robustness of the energetic arrangement of molecular frontier orbitals, we consider porphyrin, as it constitutes the main building block of each deck of PC1. In Fig. S7 the energies and forms of porphyrin frontier molecular orbital wave functions are compared for the generalized-gradient and hybrid exchange-correlation functionals PBE[2] and PBE0.[3] While the exact energetic positions of the frontier orbitals for PBE and PBE0 differ, the shape of the wave functions and their energetic ordering match for both functionals in a range of several eV around the HOMO-LUMO gap. In this sense, the energetic ordering

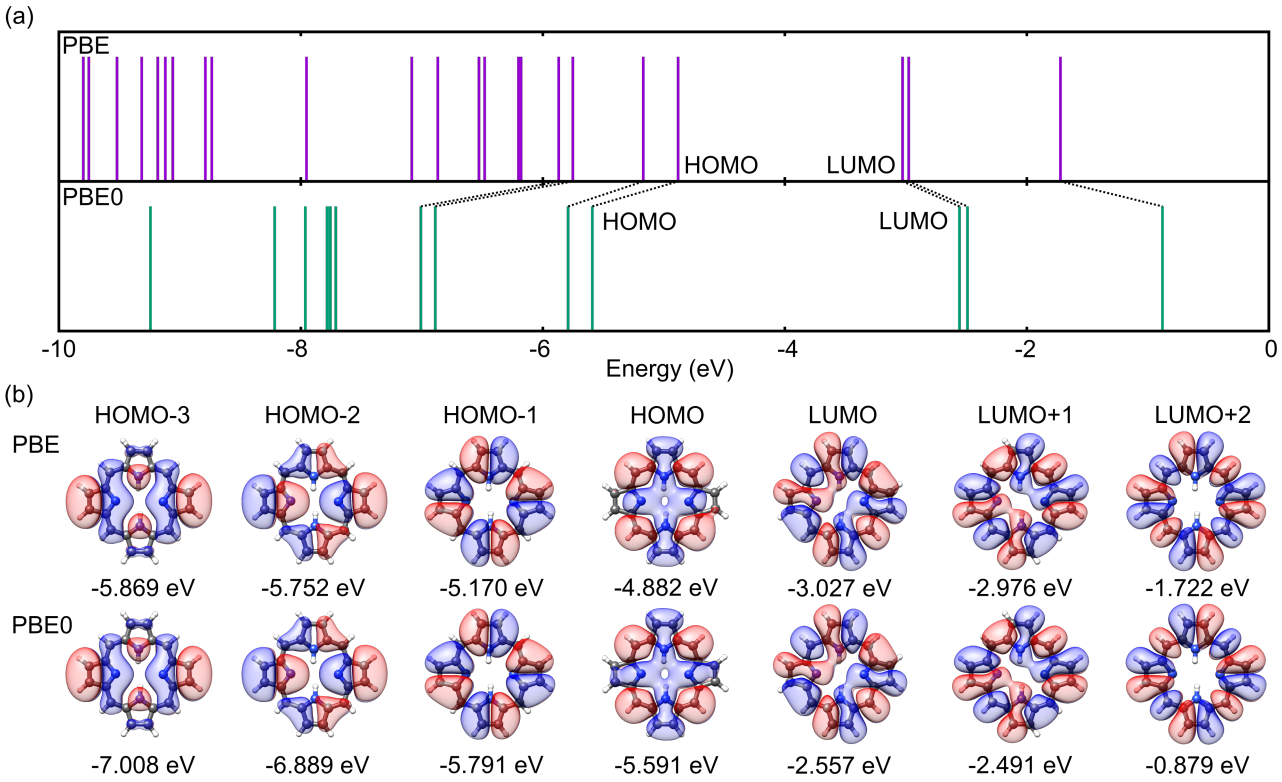

Figure S7 (a) Energies of molecular orbitals of a porphyrin molecule in the vicinity of the HOMO-LUMO gap, obtained with PBE and PBE0 exchange-correlation functionals. (b) Molecular orbital wavefunctions for HOMO-3 to LUMO+2 and their respective energies. The settings of the DFT calculations are identical to those described in the main text.

is robust with respect to the choice of DFT exchange-correlation functional, and we expect the same for the qualitative interpretation of the distance dependence of the conductance, presented in the main text.

ESI.2 Experimental

ESI.2.1 MCBJ setup

The single-molecule experiments described in the main text are performed with a MCBJ setup. The MCBJ samples are fabricated with electron-beam lithography on a flexible phosphor bronze (PB) substrate with an insulating polyimide (PI) coating. The lithographically defined gold wires are deposited with an electron beam evaporator at a thickness of 80 nm on

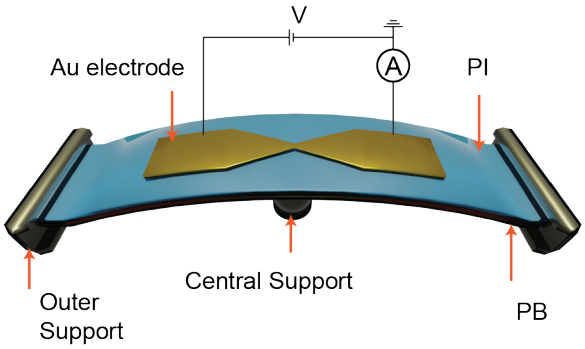

Figure S8 Schematic of a MCBJ setup.

top of a 3 nm thick titanium adhesive layer. After the lift-off process of the defined pattern, an oxygen plasma is used to create an under-cut to suspend the gold electrodes.

After the fabrication, the MCBJ sample is mounted onto the MCBJ setup for single-molecule characterization. Prior to the measurement of molecules of interest, a reference fast-breaking measurement with the clean MCBJ sample is performed. Afterwards, a molecular solution containing PC1 or ZnPC1 with a concentration from 1 to 50 μM is used for drop-casting the molecule onto the sample. The fast-breaking and electrode-distance modulation measurements are then performed, following the protocols described in Methods.

ESI.2.2 Fast-breaking measurements of ZnPC1

Fast-breaking measurements of ZnPC1 yield the results shown in Fig. S9a and S9b. Similar to the fast-breaking result for PC1, a conductance plateau at around $7 \times 10^{-6} G_0$ is observed, consistent (within the standard deviation on a logarithmic-normal scale) with previous experiments.[5] Conductance variations up to 1.5 orders of magnitude are observed in individual breaking traces, as evident from Fig. S9c. The similarity between the 2D conductance histograms of ZnPC1 and PC1 suggests that the Zn metal core has little contribution to the electric conduction, which is in agreement with previous measurements on single-porphyrin junctions.[6] In addition, comparable conductance variations in the individual traces indicate that the underlying DQI features are basically unaffected by the presence of Zn atoms.

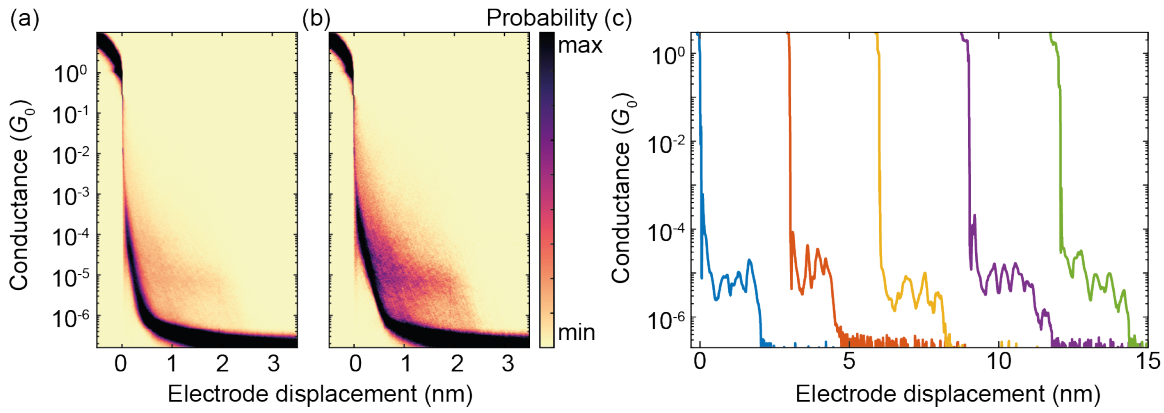

Figure S9 Fast-breaking measurements of ZnPC1. (a) 2D conductance-displacement histogram consisting of 10,000 consecutive fast-breaking traces. (b) 2D conductance-displacement histogram, constructed exclusively from molecular traces, extracted with a reference-free clustering algorithm.[4] (c) Examples of individual breaking traces, which are displaced by 3 nm for better visibility.

ESI.2.3 Electrode-displacement modulation for ZnPC1

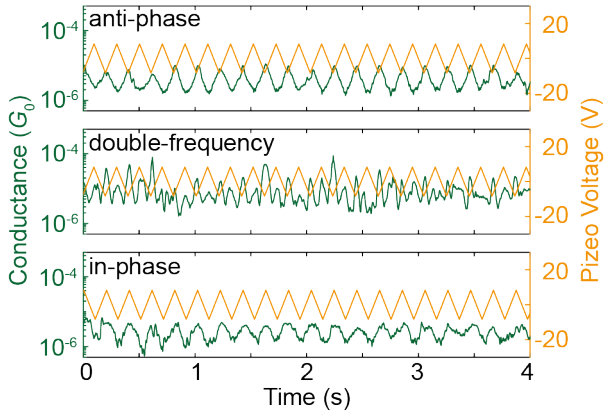

Figure S10 Electrode-displacement modulation of ZnPC1. Anti-phase, double-frequency and in-phase responses are observed with a modulation amplitude of 5 Å. The modulation is performed at 5 Hz with a duration of 15 s. Here, for clarity a zoom-in on a modulation time interval of 4 s is used.

We have performed the same electrode-displacement modulations for ZnPC1, as shown in the main text for PC1. As visible in Fig. S10, we find the same three different types of behavior, namely anti-phase, double-frequency and in-phase. This indicates the presence of a conductance dip in our electrode-displacement range, as also observed for PC1. Importantly, we find no qualitative difference between the modulation experiments with ZnPC1 and PC1. This confirms again that Zn has little influence on the DQI dips.

ESI.2.4 Higher order frequency responses

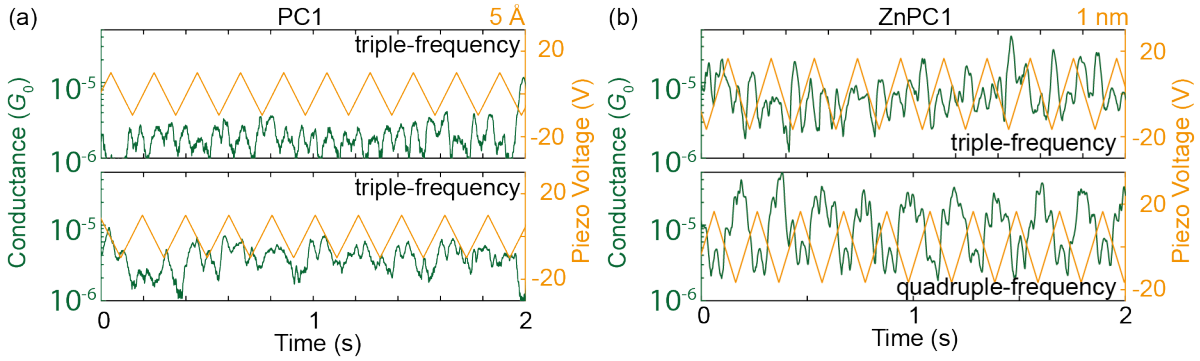

Figure S11 Higher order frequency responses of molecular junctions containing PC1 and ZnPC1. (a) Examples of triple-frequency response for PC1. The modulation setting is the same as in the main text with an amplitude of 5 Å (piezo voltage of ±10 V). (b) Examples showing higher order frequency responses for ZnPC1. The top panel displays a triple-frequency response and the bottom panel shows a quadruple-frequency response. Note that a larger modulation amplitude of 1 nm (piezo voltage of ±20 V) was used for both measurements with ZnPC1.

Further examples of higher order frequency modes are presented in Fig. S11 for PC1 and ZnPC1. For PC1 an electrode-displacement amplitude of 5 Å is used and triple-frequency behavior is observed, similar to what we describe in the main text. For ZnPC1, a larger modulation amplitude of 1 nm yields in addition to the triple-frequency mode, see the upper panel of Fig. S11b, a quadruple-frequency mode, see the bottom panel of Fig. S11b. This latter case may be attributed to a full crossing of two DQI dips, as discussed in the main text. However, the characteristic is not as clear as the triple-frequency response, and the large modulation amplitude used here may possibly induce a slipping of the molecule in the junction.

ESI.2.5 Fast-breaking measurements of PC1 at elevated voltage

In the main text we present experimental conductance data for a bias voltage of 100 mV. For completeness we have also measured the PC1 junctions at a higher bias of 250 mV. The results are shown in Fig. S12. In Fig. S12a and more clearly in Fig. S12b a conductance plateau with $G \approx 2 \times 10^{-6} G_0$ is identified. The conductance values of the plateaus at

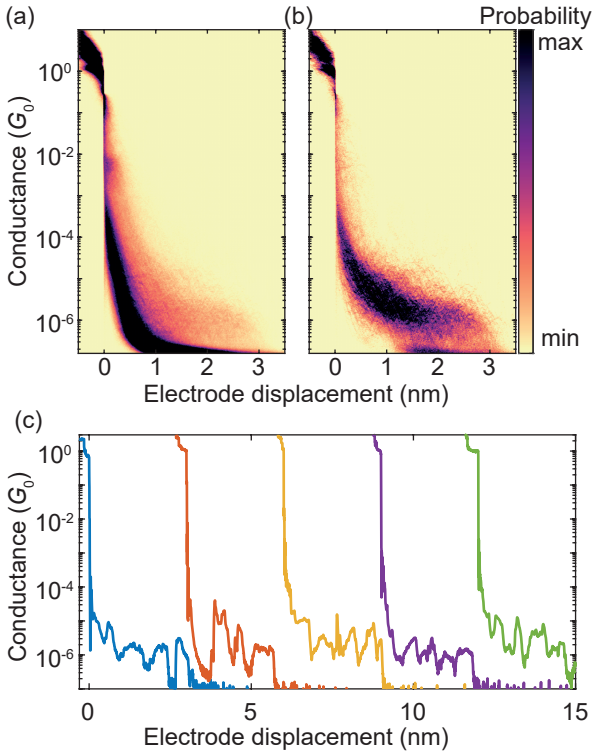

Figure S12 Fast-breaking measurements of PC1 at 250 mV. (a) 2D conductance-displacement histogram consisting of 10,000 consecutive fast-breaking traces. (b) 2D histogram containing molecular traces, extracted with the clustering algorithm. (c) Examples of individual traces, each displaced by 3 nm for better visibility, showing the oscillating behavior during the electrode separation process.

100 mV and 250 mV coincide, showing that the reported conduction properties are robust with regard to bias voltage changes. Furthermore, as shown in Fig. S12c, the behavior of the conductance-displacement curves is comparable to those reported in Fig. 6c of the main text. As before we attribute the multiple conductance oscillations to a stick-slip motion, exhibiting comparable quantum interference features at 250 mV as in the case of 100 mV. To probe the energy and voltage dependence of the transmission, the bias voltage window would need to be increased even further. Yet the PC1 single-molecule junctions become rather unstable for voltages above 500 mV at room temperature.

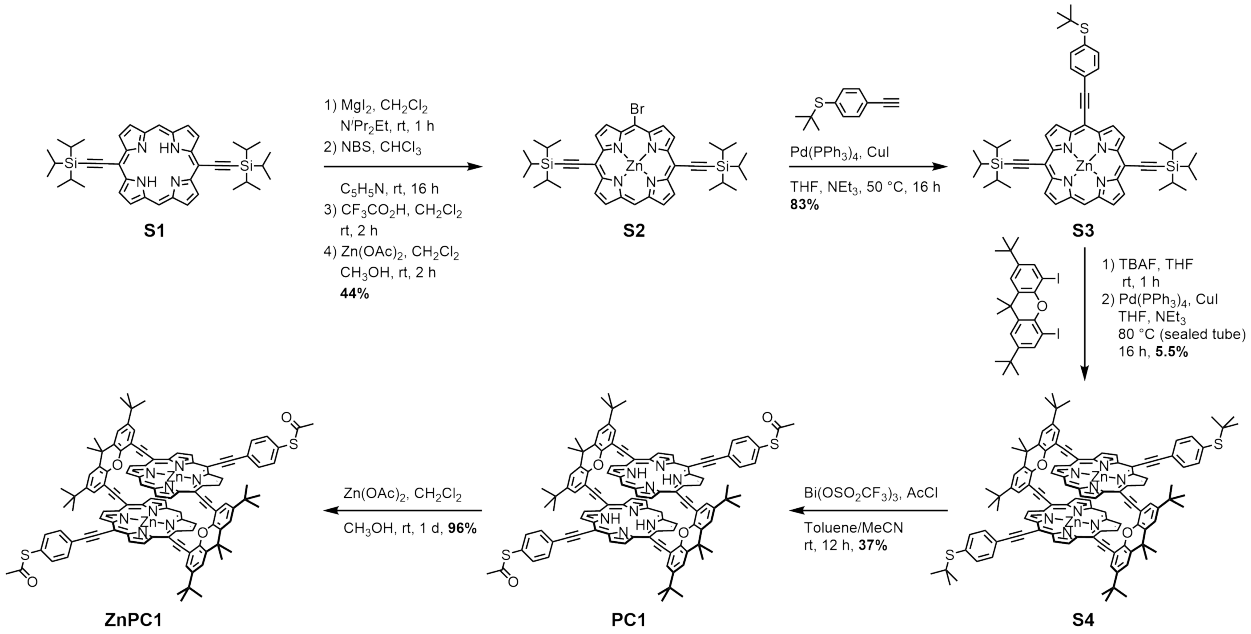

Figure S13 Synthetic overview, leading to the final products PC1 and ZnPC1.

ESI.3 Synthesis

The structures PC1 and ZnPC1, studied here, were synthesized and characterized as described in detail previously.[5] A metalation and de-metalation procedure, combining statistical bromination of S1, afforded the asymmetric porphyrin precursor S2, see Fig. S13. Subsequent palladium-mediated Sonogashira cross coupling with the anchoring group bearing phenyl ethynylene yielded the key intermediate of the synthesis, S3. Liberation of the free acetylenes enabled four-fold Sonogashira macrocyclization, yielding S4 under high dilution conditions. Bismuth triflate-promoted trans-protection of the thioethers to thioacetates gave the compound of interest, PC1, which quantitatively undergoes metalation affording ZnPC1.

References

(1) Yoshizawa, K.; Tada, T.; Staykov, A. *J. Am. Chem. Soc.* **2008**, *130*, 9406–9413.

(2) Perdew, J. P.; Burke, K.; Ernzerhof, M. *Phys. Rev. Lett.* **1996**, *77*, 3865–3868.

(3) Perdew, J. P.; Ernzerhof, M.; Burke, K. *J. Chem. Phys.* **1996**, *105*, 9982–9985.

(4) Cabosart, D.; El Abbassi, M.; Stefani, D.; Frisenda, R.; Calame, M.; van der Zant, H. S. J.; Perrin, M. L. *Appl. Phys. Lett.* **2019**, *114*, 143102.

(5) Zwick, P.; Hsu, C.; El Abbassi, M.; Fuhr, O.; Fenske, D.; Dulić, D.; van der Zant, H. S. J.; Mayor, M. *J. Org. Chem.* **2020**, *85*, 15072–15081.

(6) El Abbassi, M.; Zwick, P.; Rates, A.; Stefani, D.; Prescimone, A.; Mayor, M.; van der Zant, H. S. J.; Dulić, D. *Chem. Sci.* **2019**, *10*, 8299–8305.